Title

3D spatially encoded and accelerated TE-averaged echo planar spectroscopic imaging in healthy human brain

Journal

NMR in Biomedicine, 29(3)

ISSN

0952-3480

Authors

Iqbal, Zohaib
Wilson, Neil E
Thomas, M Albert

Publication Date

2016-03-01

DOI

10.1002/nbm.3469

Peer reviewed

Research article

NMR IN BIOMEDICINE

Received: 16 June 2015, Revised: 17 November 2015, Accepted: 23 November 2015, Published online in Wiley Online Library: 8 January 2016

(wileyonlinelibrary.com) DOI: 10.1002/nbm.3469

3D spatially encoded and accelerated TE-averaged echo planar spectroscopic imaging in healthy human brain

Zohaib Iqbal, Neil E. Wilson and M. Albert Thomas*

Several different pathologies, including many neurodegenerative disorders, affect the energy metabolism of the brain. Glutamate, a neurotransmitter in the brain, can be used as a biomarker to monitor these metabolic processes. One method that is capable of quantifying glutamate concentration reliably in several regions of the brain is TE-averaged ^{1}H spectroscopic imaging. However, this type of method requires the acquisition of multiple TE lines, resulting in long scan durations. The goal of this experiment was to use non-uniform sampling, compressed sensing reconstruction and an echo planar readout gradient to reduce the scan time by a factor of eight to acquire TE-averaged spectra in three spatial dimensions. Simulation of glutamate and glutamine showed that the 2.2–2.4 ppm spectral region contained 95% glutamate signal using the TE-averaged method. Peak integration of this spectral range and home-developed, prior-knowledge-based fitting were used for quantitation. Gray matter brain phantom measurements were acquired on a Siemens 3 T Trio scanner. Non-uniform sampling was applied retrospectively to these phantom measurements and quantitative results of glutamate with respect to creatine 3.0 (Glu/Cr) ratios showed a coefficient of variance of 16% for peak integration and 9% for peak fitting using eight-fold acceleration. *In vivo* scans of the human brain were acquired as well and five different brain regions were quantified using the prior-knowledge-based algorithm. Glu/Cr ratios from these regions agreed with previously reported results in the literature. The method described here, called accelerated TE-averaged echo planar spectroscopic imaging (TEA-EPSI), is a significant methodological advancement and may be a useful tool for categorizing glutamate changes in pathologies where affected brain regions are not known *a priori*. Copyright © 2016 John Wiley & Sons, Ltd.

Keywords: TE-averaged; compressed sensing; non-uniform sampling; human brain; 3D spectroscopic imaging; glutamate quantitation

INTRODUCTION

It is well known that several pathologies cause metabolic changes in the human brain. In some instances, these abnormalities are detected before any anatomical changes occur and can therefore be used as markers for detection. An effective method for studying metabolic differences *in vivo* is ^{1}H magnetic resonance spectroscopy (MRS). In particular, spectroscopic imaging (SI) acquires spectra from several spatial locations in a single scan (1), allowing for comparisons between different regions of the brain. Glutamate (Glu), a neurotransmitter, plays an important role in brain processes and is also known to be a marker of interest for several neurodegenerative diseases (2,3). One of the main concerns in neurodegenerative conditions is glutamate excitotoxicity, which results from a dysfunctional energy metabolism in the brain. This type of process causes continuous stimulation of glutamate receptors, which eventually leads to nerve cell death (4). These receptors have become interesting targets for different drugs and neuroprotective effects have been reported by blocking these receptors (5). Quantifying glutamate provides useful insight into the energy metabolism of the brain and greatly aids in the investigation of different pathologies.

Due to severe spectral overlap with glutamine (Gln) and gamma-aminobutyric acid (GABA), quantitation of Glu is difficult using a typical one-dimensional (1D) spectroscopy sequence such as point-resolved spectroscopy (PRESS) (6). One method that overcomes this problem is TE-averaged point-resolved spectroscopy (PRESS-2D J) (7). This method uses the data acquired by a two-dimensional (2D) J-resolved spectroscopy (JPRESS) (8)

* *Correspondence to: M. A. Thomas, Department of Radiological Sciences, University of California Los Angeles, 10945 Le Conte Avenue, Suite #3371, Los Angeles, California, USA, 90095.*
E-mail: athomas@mednet.ucla.edu

Z. Iqbal, N. E. Wilson, M. A. Thomas
Department of Radiological Sciences, University of California Los Angeles, USA

Abbreviations used: *1D, one-dimensional; 2D, two-dimensional; 3D, three-dimensional; 5D EP-JRESI, five-dimensional echo planar J-resolved spectroscopic imaging; 8x, eight-fold acceleration; Ala, alanine; Asc, ascorbic acid; Asp, aspartic acid; BG, basal ganglia; Ch, total choline (phosphocholine, glycerylphosphorylcholine and choline); Cr3.9, creatine at 3.9 ppm; Cr, Creatine at 3.0 ppm; CRLB, Cramér–Rao lower bound; CS, compressed sensing; CSDE, chemical shift displacement error; CV, coefficient of variance; FG, frontal gray matter; FOV, field of view; FW, frontal white matter; GABA, gamma-aminobutyric acid; Glc, glucose; Gln, glutamine; Glu, glutamate; Glx, glutamine and glutamate; Gly, glycine; JPRESS, J-resolved spectroscopy; Lac, lactate; MANGO, Metabolite Assessment aNd Graphical Overlay; mI, myo-inositol; NAAG, N-acetyl-aspartyl-glutamate; NAA, N-acetyl aspartate; NUS, non-uniform sampling; Pe, phosphoethanolamine; PG, parietal gray matter; PRESS-2D J, TE-averaged point-resolved spectroscopy; PRESS, point-resolved spectroscopy; ProFit, prior knowledge fitting; PW, parietal white matter; RMSE, root-mean-square error; Scy, scyllo-inositol; SI, spectroscopic imaging; Tau, taurine; TEA-EPSI, TE-averaged echo planar spectroscopic imaging; Thr, threonine; TV, total variation; VAPOR, seven-pulse water suppression scheme.*

experiment, where several different TEs are acquired in order to exploit the J modulation of different metabolites. JPRESS spreads these signals over a second spectral dimension, whereas PRESS-2D J averages these signals. Due to the phase evolution along the indirect dimension (t_1), averaging these spectra can result in either constructive or destructive addition of metabolites. This leads to the enhancement of certain metabolite signals and the suppression of others, which can be viewed through simulation of the spectra. Therefore, depending on the TEs that are chosen and averaged, certain metabolites that are usually difficult to detect can be highlighted and quantified (9–11). This technique has already been used *in vivo* to study the Human Immunodeficiency Virus (12), Alzheimer's disease (13), multiple sclerosis (14), age differences in the brain (15) and familial risk of depression (16).

Unfortunately, one of the limitations of this technique combined with SI is the long acquisition time (17,18). Our group has recently developed the five-dimensional echo planar J-resolved spectroscopic imaging (5D EP-JRESI) technique (19), which is capable of acquiring J-resolved spectra from three spatial dimensions (3D) in a clinically feasible scan time (20 minutes). This method uses an echo planar readout to acquire a spatial and spectral dimension simultaneously (20,21). For further acceleration, a non-uniform sampling (NUS) scheme applied across the incremented dimensions (k_y, k_z, t_1) along with compressed sensing (CS) reconstruction (22) is also implemented. Applying NUS along the incremented dimensions is a method that has been used in high-resolution NMR along the indirect spectral dimensions to accelerate scan time (23–26). The major difference between applications in high-resolution NMR and the 5D EP-JRESI method is that instead of applying NUS along spectral dimensions only, the sampling mask is also applied in the k-space domains. A major goal of this work is to demonstrate that a new technique, called accelerated TE-averaged echo planar spectroscopic imaging (TEA-EPSI), is capable of obtaining PRESS-2D J spectra from three spatial dimensions reliably in a clinically feasible scan time. TEA-EPSI is applied to quantify Glu in phantom as well as in healthy human brain.

METHODS

Simulation

GAMMA simulated (27) JPRESS basis sets were created for Glu and Gln using the following parameters: TE_{min} = 30 ms, $\Delta TE = 1$ ms, t_1 points = 64, t_2 points = 256, direct spectral bandwidth (SBW) = 1190 Hz and assuming ideal RF pulses. $\Delta TE = 1$ ms and t_1 points = 64 were chosen to mitigate signal loss due to T_2 decay when moving into *in vivo* studies. Since the Siemens 3 T Trio scanner was used for all phantom and *in vivo* acquisitions, the B_0 for simulation was set appropriately. A maximum echo-sampling scheme (28), where only one t_1 increment was added between the two 180° pulses, was used. In post-processing, the second t_1 increment was added as a linear phase multiplication in the F_2, t_1 domain (29), resulting in an indirect spectral bandwidth of ±250 Hz. Since *in vivo* T_2 values are not well known in the literature for Glu and Gln, T_2 was assumed to be 90 ms for both metabolites. A point-resolved spectroscopy (PRESS) (6) spectrum was obtained by taking the first t_1 line and was compared with the TE-averaged (PRESS-2D J) spectrum, where all of the t_1 lines were averaged. Noise was simulated as 1–2% of the total Glu and Gln signal for each t_1 line. Gln concentration was simulated as one third of the Glu concentration to replicate *in vivo* conditions.

Sampling mask

A non-uniform sampling mask was applied in the incremented dimensions (k_y, k_z, t_1). The pulse sequence diagram for the 5D EP-JRESI displayed in Figure 1 shows the non-uniformly sampled dimensions using red arrows. The sampling mask used is based on the following exponential (23) probability density function:

$$P(k_y, k_z, t_1) = \exp\left\{-\frac{|k_y|}{2} - \frac{|k_z|}{2} - t_1\right\} \quad [1]$$

where $P(k_y, k_z, t_1)$ is the probability of sampling a point in the three-dimensional volume, $k_y = [-8, -7, -6, \ldots, 7]$, $k_z = [-4, -3, -2, \ldots, 3]$ and $t_1 = [0, 1, 2, \ldots, 63]$. These values are chosen based on the resolution along the k_y, k_z and t_1 dimensions, which is 16, 8 and 64. This type of mask puts an emphasis on sampling points with higher signals, meaning the central part of *k*-space and earlier t_1 points. The sampling mask used for the sequence can be seen in Figure 2, where the sampled points are in copper.

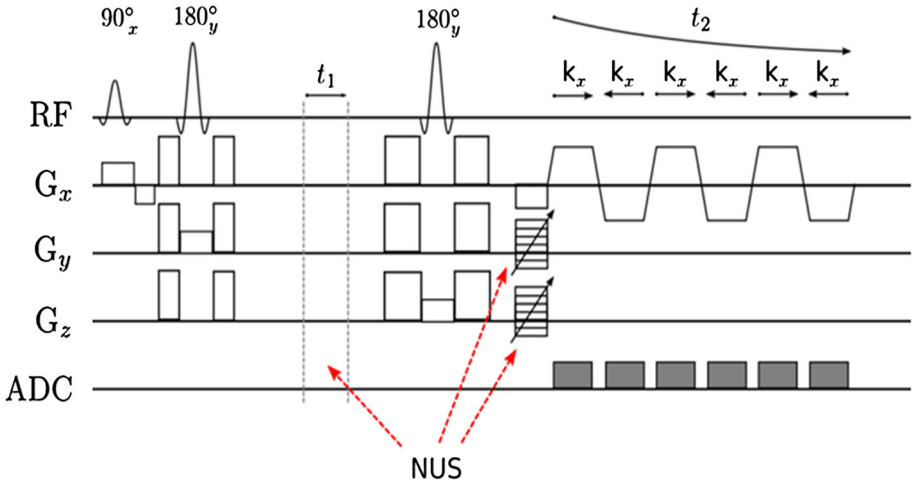

Figure 1. The pulse diagram for the 5D EP-JRESI sequence is shown. Non-uniform sampling is applied in the t_1 dimension and the phase-encoding (k_y,k_z) dimensions indicated by the red arrows. An echo planar readout is used to acquire (k_x,t_2) for each increment simultaneously.

NMR IN BIOMEDICINE

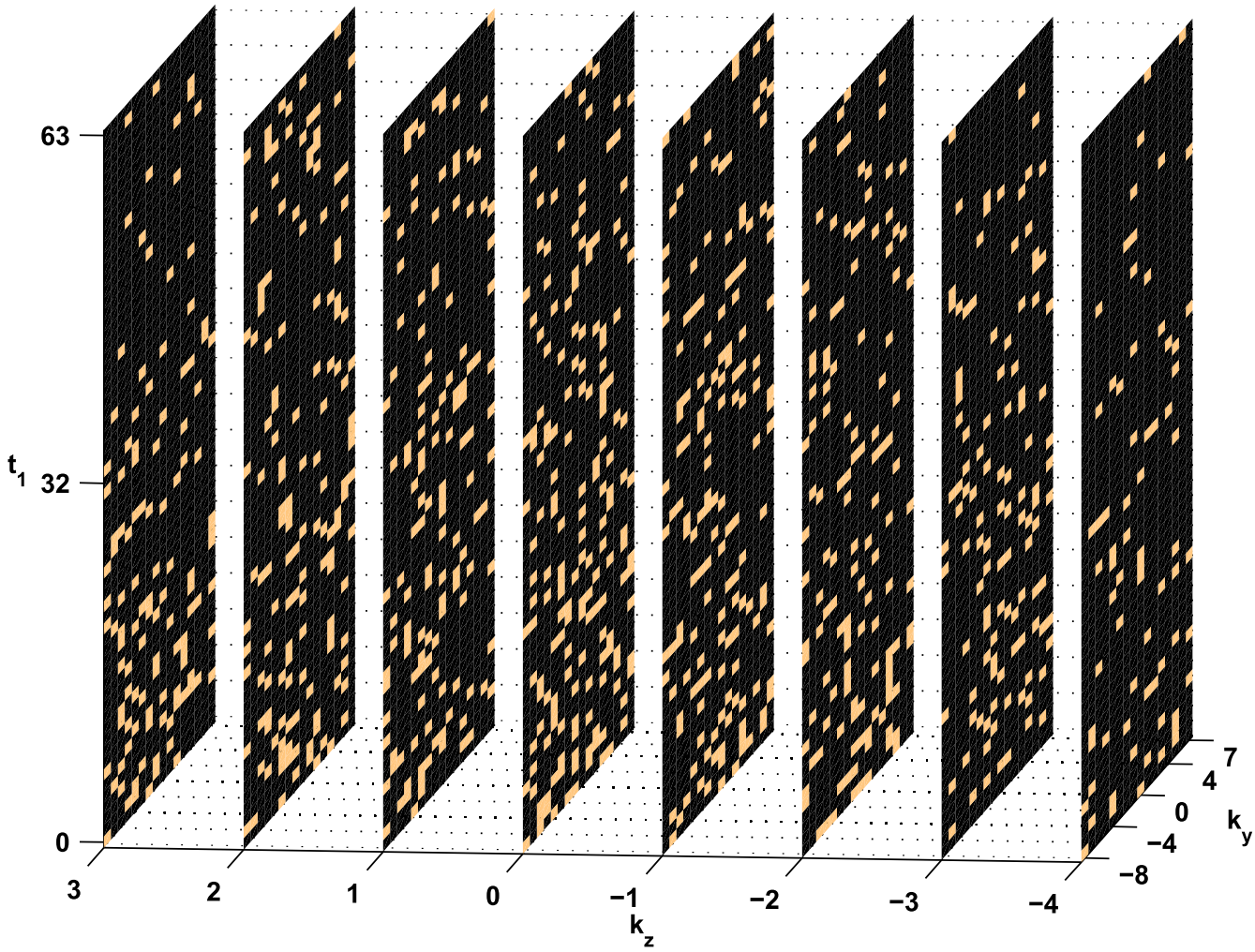

Figure 2. The 8× sampling mask used for the 5D EP-JRESI acquisition is displayed. The copper points are sampled, whereas the black points are not. The non-uniform sampling is applied in the incremented dimensions, so the mask is displayed for the (k_y,k_z,t_1) volume.

Phantom

12 measurements of a brain phantom with gray matter metabolite concentrations (30) were acquired on the Siemens 3 T Trio scanner using a fully sampled 5D EP-JRESI sequence. The parameters used for acquisition were the same as those used for simulation. The phantom measurement used a TR of 1200 ms, a field of view (FOV) of 16 × 16 × 12 cm^3 and a spatial resolution of 1 × 1 × 1.5 cm^3. The masking scheme shown in Figure 2 was applied retrospectively for an acceleration factor of eight (8×) and was processed as described below to reconstruct the data. In order to make a fair time equivalent (Time Eq. TEA) comparison, equally spaced t_1 points from the fully sampled phantom data were averaged together. The eight t_1 points included in this average were $t_1 = [1, 9, 17, 25, 33, 41, 49, 57]$ and these were averaged point-by-point for each spatial location. For quantitation, 20 voxels were used from the two central slices for each TE-averaged scan. The fully sampled TE-averaged group that averaged over all 64 t_1 points (Full TEA-EPSI), the time-equivalent TE-averaged group that averaged over eight t_1 points (Time Eq. TEA) and the accelerated TE-averaged group, which was undersampled and reconstructed and averaged over 64 t_1 points (8× TEA-EPSI), were assessed using both peak integration and prior-knowledge-based fitting.

In order to determine the effects of reconstruction on quantitation, a normalized root-mean-square error (RMSE) between the Full TEA-EPSI and the 8× TEA-EPSI was calculated. This RMSE used the metabolite concentrations from the prior-knowledge fitting of the 20 voxels from each phantom scan. The normalized RMSE was determined by the following equation:

$$RMSE = \frac{\sqrt{\frac{1}{20}\sum \left(c_{full} - c_{8x}\right)^2}}{\bar{c}} \quad [2]$$

where c_{full} is the Full TEA-EPSI metabolite concentration and c_{8x} is the 8× TEA-EPSI metabolite concentration. This RMSE was normalized to the mean of the Full TEA-EPSI data ($\bar{c}$).

In vivo

Ten healthy adults (mean age = 25 years) were scanned on a Siements 3 T Trio with an 8-channel head receive coil using the same parameters described above. For *in vivo* scans, the FOV was set to 24 × 24 × 12 cm^3.These scans were acquired using 8x NUS for a total acquisition time of about 20 minutes for the metabolite scan (with water suppression (31)) and about 3 minutes for the water reference scan. The water scan was

acquired using the first t_1 point only with a single average. Processing was performed as described below to obtain the TEA-EPSI data, $u(x, y, z, F_{TE})$, where the F_{TE} dimension contains the TE-averaged spectra in the frequency domain. Five locations (frontal white, mid-frontal gray, basal ganglia, parietal white and mid-parietal gray) were identified for each volunteer and quantified. The white matter voxels were chosen to the left of the gray matter voxels in the frontal and parietal regions. The basal ganglia region was chosen left of the ventricles.

Processing

The non-uniformly sampled 5D EP-JRESI data were extracted and reconstructed in MATLAB using the total variation (TV) method described in (19). The 5D EP-JRESI sequence utilizes an exponential sampling scheme in the incremented dimensions (k_y, k_z, t_1), as described above, to accelerate the scan by a factor of eight (8x) or more. Before reconstruction, the second t_1 increment was added as described above. The following optimization problem is solved using a modified split Bregman (32) algorithm to reconstruct the data:

$$\min_u TV(u) \quad \text{s.t.} \quad \|R\mathcal{F}u - f\|_2^2 < \sigma^2 \qquad [3]$$

where u denotes the 5D reconstructed data $u(x, y, z, F_2, F_1)$, R the sampling mask, $\mathcal{F}$ the Fourier transform operator applied across (k_y, k_z, t_1), f the undersampled data $f(x, k_y, k_z, F_2, t_1)$and σ^2 an estimate of the noise variance. This reconstruction was performed on a coil-by-coil basis, so the final reconstructed data are $u(x, y, z, c, F_2, F_1)$, where c is the number of coils. Klose's correction was applied for eddy-current corrections (33) after reconstruction based on the water reference scan.

In order to combine the coils, each voxel in (x, y, z, c) had frequency-drift and phase corrections applied in F_2, F_1. These corrections were based on the GAMMA simulated basis set of the singlets (NAA, Cr and Ch) and were implemented as a non-linear least-squares optimization problem similar to how the new Prior Knowledge Fitting (ProFit) algorithm implements pre-processing and peak fitting (34). The lsqnonlin function in MATLAB was first used to acquire the correct frequency-drift and line-broadening corrections based on the known peak locations of the singlets. The frequency-drift corrections were applied to the experimental data and the line-broadening corrections were applied to the basis set. The lsqnonlin function was then used again to obtain the zero-order phase correction for the data. In both cases, the minimization of the sum of squares problem was similar:

$$\min_p \|\mathcal{B}_s - g(p)\|_2^2 \qquad [4]$$

where $g(p)$ represents the experimental data as a function of different parameters: frequency drift, line broadening or phase values. $\mathcal{B}_s$ is the partial basis function including only the singlets. Both matrices, $\mathcal{B}_s$ and $g(p)$, were truncated to the singlet regions. This method for coil combination took approximately 20 seconds for a single voxel using a 32 GB RAM computer with an Intel i7 core processor. Of course, the coil combination time depends greatly on the number of coil elements used for data acquisition.

The coils were summed so that the resulting data matrix, $u(x, y, z, F_2, F_1)$, could easily be brought into $u(x, y, z, F_2, t_1)$ through an inverse Fourier transformation along F_1. Afterwards, the matrix was averaged over the t_1 dimension to obtain the TEA-EPSI data, $u(x, y, z, F_{TE})$, where F_{TE} is the TE-averaged spectral dimension.

Quantitation

The phantom data were quantified using both peak integrals and an in-house MATLAB-based, prior-knowledge fitting program. In contrast, the *in vivo* data were quantified only using the prior-knowledge fitting algorithm. For peak integration, the following metabolites were quantified: N-acetylaspartate (NAA), Glu, creatine 3.0 (Cr), total choline (Ch) and myo-Inositol (mI). The peak integration ranges used for this method can be seen in Table 1.

The coefficient of variance was determined along with the mean metabolite values and was calculated as

$$CV = \frac{std}{mean} \times 100\% \qquad [5]$$

where std. is the standard deviation. For the phantom data, the CV and mean were calculated over all 12 phantom measurements ($n = 240$). For *in vivo* data, the CV and mean were calculated over each brain region for all 10 healthy volunteers ($n = 10$).

Several one-dimensional (1D) quantitation programs utilizing basis spectra already exist (35–38), however an alternative quantitation program was written to implement fitting easily into the existing MATLAB pipeline. The program fits the TE-averaged data in the frequency domain and is based on the linear least-squares optimization problem:

$$\min_w \|\mathcal{B}w - F\|^2 \qquad [6]$$

where $\mathcal{B}$ is the TE-averaged basis spectrum for each metabolite, w is the weighting for each metabolite and F is the acquired TE-averaged spectrum. By normalizing the weighting factors to Cr, it is possible to obtain metabolite ratios. The linear least-squares optimization problem is solved using (39):

$$w_{ls} = \left(\mathcal{B}^T\mathcal{B}\right)^{-1}\mathcal{B}^T F \qquad [7]$$

where w_{ls} is the optimized metabolite weighting factors. Prior to solving this optimization problem, a line-broadening factor based on the experimental line width of NAA is applied to the TE-averaged basis set. A total of 21 metabolites were included in the basis set, however only NAA, Glu, Ch and mI are reported with respect to Cr for phantom. The other metabolites included were alanine (Ala), ascorbic acid (Asc), aspartic acid (Asp), creatine 3.9 (Cr3.9), GABA, glucose (Glc), Gln, glycine (Gly), lactate (Lac), NAAG, phosphoethanolamine (Pe), scyllo-Inositol (Scy),

Table 1. The list of metabolite peak integration ranges. All of the peak integrals used 0.2 ppm ranges.

Metabolite	ppm range
NAA	(1.9, 2.1)
Glu	(2.2, 2.4)
Cr	(2.9, 3.1)
Ch	(3.1, 3.3)
mI	(3.4, 3.6)

taurine (Tau) and threonine (Thr). For *in vivo*, only NAA, Glu, and Ch with respect to Cr are reported. In general, the TE-averaged method is not a reliable technique to quantify lower concentration metabolites.

Normally, a quality control metric such as the Cramér–Rao lower bound (CRLB) (40) is determined for each metabolite. This metric is highly dependent on the noise level of the experimental data. It is still not well understood how a denoising algorithm such as TV affects the CRLB values and this is the reason it is not yet included in the algorithm. The fitting program, called Metabolite Assessment aNd Graphical Overlay (MANGO), is also capable of graphing the fit results. The residual in the fit results is calculated as the absolute difference between the fit and the actual data. MANGO takes approximately 2–3 seconds to fit a voxel on a 32 GB RAM computer with an i7 core processor, making it ideal for automated fitting for a large number of voxels.

Since MANGO is a new prior-knowledge fitting method, a Monte Carlo simulation was performed in order to determine the goodness of fit of this algorithm as noise levels varied. A TE-averaged spectrum was simulated using the following metabolite ratios with respect to Cr3.0: NAA = 1.274, Ch = 0.438, Glu = 1.561, Gln = 0.511, mI = 0.48 and low concentrations of several other metabolites. A total of 4000 different noise levels were used and noise was measured as the SNR between the NAA singlet (1.9–2.1 ppm) and a noisy region (5.66–5.86 ppm). An emphasis was placed on SNR values below 50, which comprised 95% of the 4000 noise levels. After noise was introduced, the spectra were quantified using MANGO and compared with the known metabolite ratios.

RESULTS

Simulation

The comparison between the simulated PRESS and TE-averaged spectra can be seen in Figure 3.

Glu and Gln concentrations were set to expected physiological conditions, meaning Gln was weighted as one third of the Glu signal. It is clear that the overlap between the two metabolites appears much more severe in the PRESS spectrum. The peak integration range chosen, 2.2–2.4 ppm, contained 11% Gln in the PRESS simulated spectrum and 3% Gln in the TE-averaged spectrum. The amount of Gln signal in this area would be very difficult to differentiate from noise, which is 1–2% of the Glu signal in the simulation.

The Monte Carlo simulation results of Glu and NAA can be seen in Figure 4.

The other major metabolites (Gln, Ch and mI) follow similar trends to the displayed results, where lower SNR spectra (SNR less than 10) have large CV values. Glu does not exceed a CV of 20% until the SNR is approximately 10, indicating that this is the SNR limit for accurate fitting results. NAA, which is further away from the noise floor, does not reach a CV of 20% until the SNR is about 5. In general, metabolites further from the noise floor (NAA and Ch) have a much lower limit than metabolites closer to the noise floor (Glu, Gln and mI). It is important to note that SNR values *in vivo* are typically much higher than the limit for Glu, even before reconstruction.

Phantom

Table 2 shows the results for the phantom quantitation. Scaling of the integrals of the singlets and multiplets was performed based on the number of protons in each peak integration range. Glu reproducibility is shown for both quantitation methods, where the CV is 16% for 8× acceleration using peak integration and 9% for 8× acceleration using MANGO fitting. Comparing the 8× TEA-EPSI results with a time-equivalent scan (Time Eq. TEA) shows that Glu CV values were lower for both peak integration and MANGO fitting using the 8× method. The normalized RMSE results can be seen in Table 3. The table gives the RMSE for each phantom scan calculated from Equation [2] and shows that the NUS and reconstruction did not change quantitation results greatly. The only case where this was not true was for Phantom 3, where spectral quality may have impacted the comparison. Nonetheless, Phantom 3 was included in the overall quantitation results with minimal negative impact on the mean and CV values.

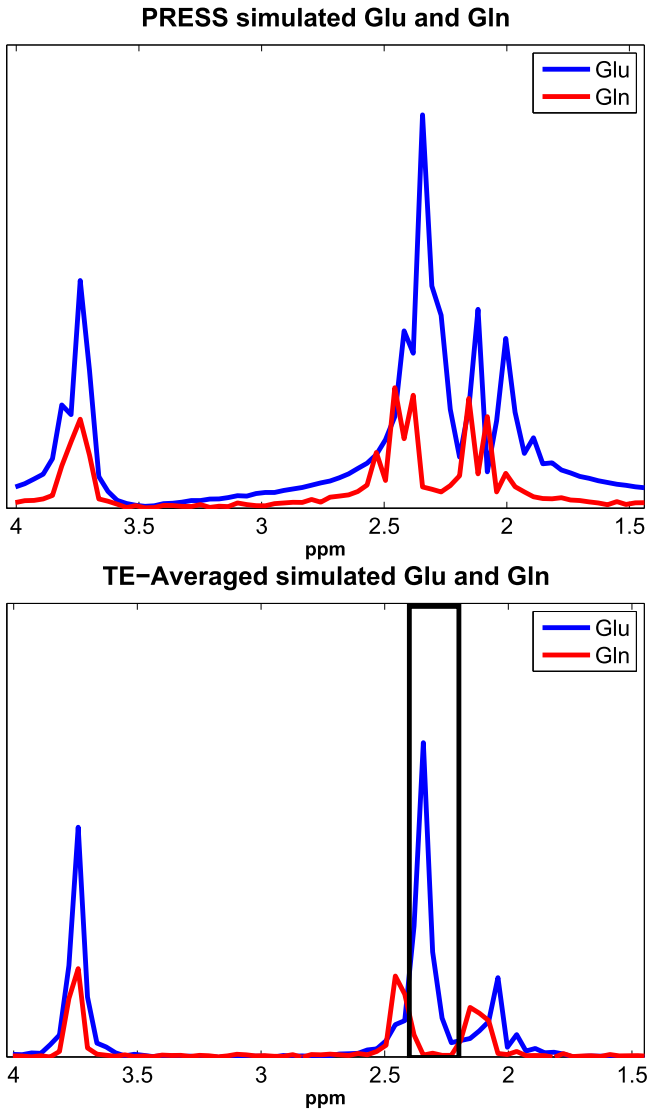

Figure 3. Simulation of PRESS and TE-averaged glutamate (blue) and glutamine (red) spectra. Gln concentration was set to one third of the Glu concentration to mimic physiological conditions. The black box represents the area for peak integration used for quantitation, 2.2–2.4 ppm, where 95% of the total signal belongs to Glu. For the PRESS simulation, only 86% of the signal in this area belongs to Glu.

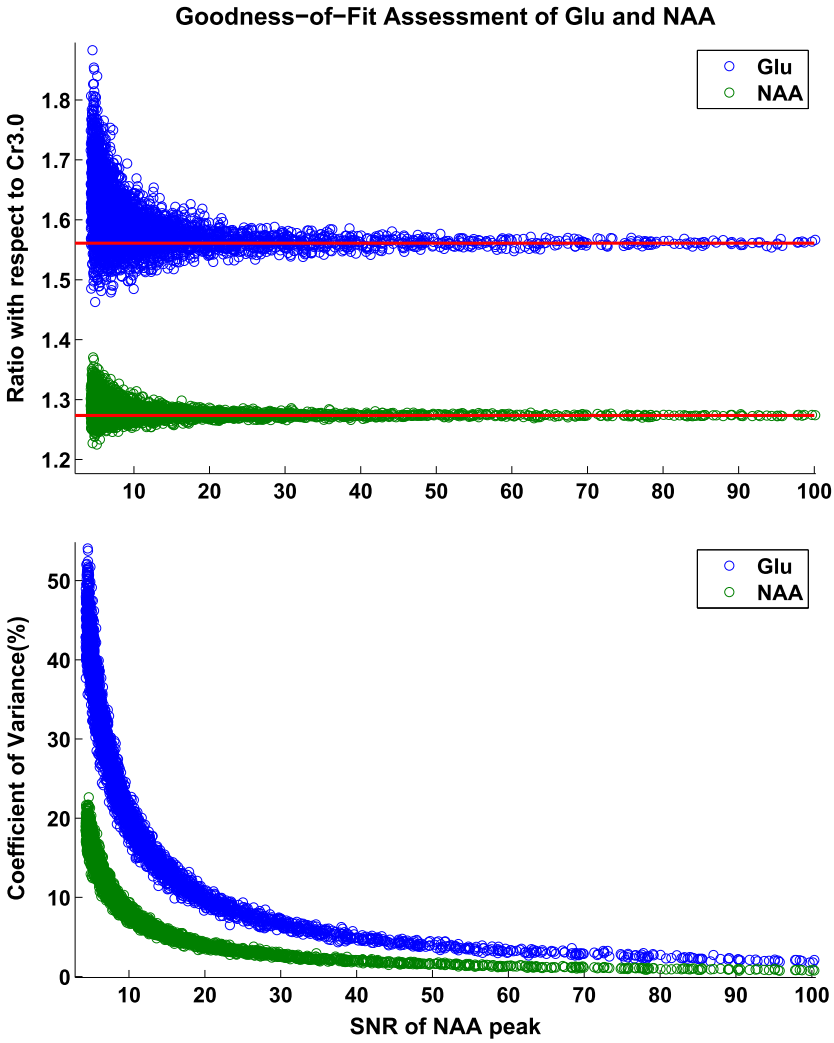

Figure 4. Monte Carlo simulation results of glutamate (blue) and NAA (green) are displayed. Metabolite ratios are displayed in the top panel, where the actual ratios with respect to Cr3.0 are shown as a red line for each metabolite. Coefficients of variance with respect to the actual ratios are shown in the bottom panel.

Table 2. Mean metabolite ratios, as well as coefficients of variance as a percentage with respect to Cr, for both fully sampled and retrospectively undersampled phantom scans. Quantitation of a time-equivalent scan using only eight t_1 lines, Time Eq. TEA, is also shown. A total of 20 voxels were used from multiple slices from each scan (12 scans total), resulting in $n = 240$. All peak integrals were scaled to account for proton number.

	NAA/Cr	Glu/Cr	Ch/Cr	mI/Cr
Phantom – Integrals				
Actual concentration	1.34	1.79	0.215	0.629
Full TEA-EPSI integrals	1.52 (6.8%)	1.43 (13%)	0.266 (9.0%)	0.568 (11%)
Time Eq. TEA integrals	1.54 (10%)	1.71 (21%)	0.273 (7.7%)	0.625 (24%)
8× **TEA-EPSI integrals**	1.58 (6.8%)	1.39 (16%)	0.270 (9.0%)	0.484 (17%)
Phantom – MANGO Fitting				
Full TEA-EPSI fit	1.47 (10%)	1.57 (11%)	0.375 (21%)	0.704 (13%)
Time Eq. TEA fit	1.37 (18%)	1.94 (18%)	0.361 (28%)	0.698 (30%)
8× **TEA-EPSI fit**	1.48 (10%)	1.53 (8.8%)	0.369 (22%)	0.582 (15%)

In vivo

Reconstructed NAA and Glu metabolite maps can be seen in Figure 5 alongside two axial slices from a 20 year old healthy volunteer. The axial slices chosen are representative of the two central slices from the PRESS localization box but do not detail the TEA-EPSI slices entirely, due to the difference in slice thickness for each acquisition (MRI = 1.5 mm and TEA-EPSI =1.5 cm). The metabolite maps were created using peak integration values instead of MANGO fit values. Fitting is inaccurate for lower

Table 3. The root-mean-square errors using MANGO fitting for each metabolite. 20 voxels were used from each phantom scan to determine the RMSE of the 8× TEA-EPSI fit results with the fully sampled TE-averaged fit results.

Peak RMSE (Decibel Scale)												
Phantom #	1	2	3	4	5	6	7	8	9	10	11	12
NAA	-22.80	-19.01	-15.64	-28.35	-30.31	-32.75	-25.46	-30.47	-20.25	-23.24	-28.13	-23.95
Glu	-13.49	-12.59	-7.49	-25.68	-22.40	-21.16	-23.58	-24.86	-16.19	-12.55	-19.46	-17.56
tCh	-18.44	-15.17	-9.97	-24.71	-20.29	-27.11	-25.96	-24.93	-17.15	-14.51	-21.73	-19.20
mI	-12.60	-10.66	-9.08	-18.38	-17.01	-18.58	-16.75	-14.01	-14.17	-11.66	-12.76	-12.21

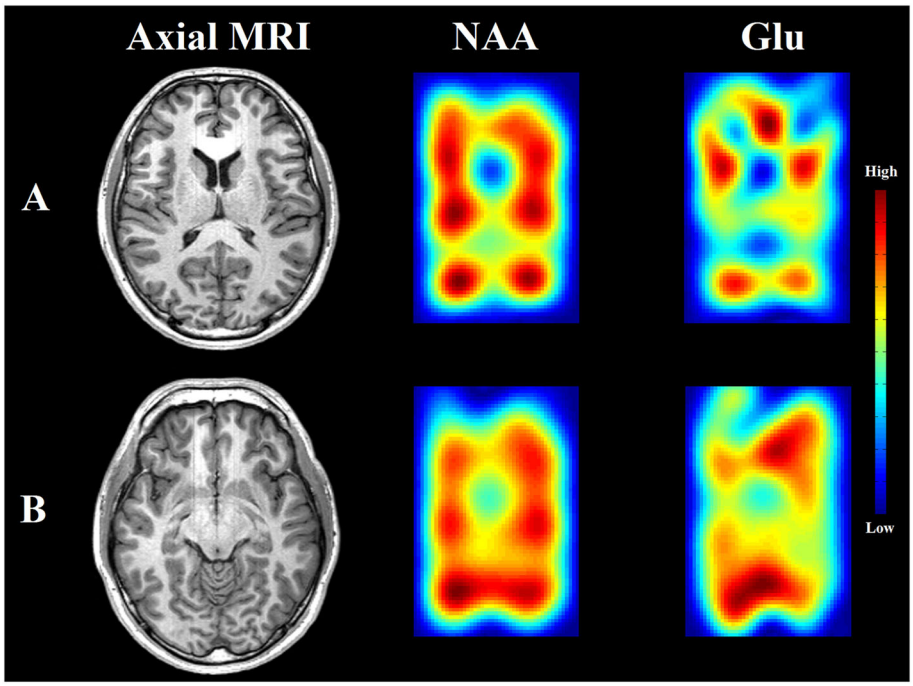

Figure 5. Metabolite maps (NAA and Glu) from a healthy volunteer (age = 20 years) are shown from the two representative slices displayed in A and B. Blue represents low signal intensity and red represents high signal intensity on the NAA and Glu maps. The metabolite maps were originally 16 × 16 but are scaled up for display purposes. The blue circles in the middle of the metabolite maps display the ventricles, which have a lack of metabolite signal.

quality regions (ventricles) and projecting all of the MANGO values led to low quality maps. The peak integral maps were originally 16 × 16 resolution, however zero-filling was applied to increase resolution for display purposes. After zero-filling, the maps were truncated to the PRESS localization box, since no other signal was present, and finally were displayed next to the MRI slices. Blue represents a lack of signal intensity and red represents high signal intensity. In Figure 5A, the gray matter shows increased Glu signal and a lack of signal where the ventricles are located. This is an expected result, since the ventricles contain mostly water and have minimal metabolite signal. Figure 6 displays the 1D TE-averaged spectra from two central slices in the same healthy volunteer shown in Figure 5. The red (C) shows the superior slice, as seen from the sagittal MRI in Figure 6A and the coronal MRI in Figure 6B, and the green (D) shows the inferior slice. Once again, spectral quality is much lower in the regions containing the ventricles, as well as in some anterior voxels. Some chemical shift displacement artifacts are also noticeable along the edges. However there are many high-quality voxels present, especially in the parietal and occipital regions. Figure 7 shows an example of MANGO fitting. Overall, the signal of the residual was low and of the same order of magnitude as the noise in most cases. However, residuals were noticeably higher in the mI region when water suppression was not optimal, which greatly increased the variation in mI for several locations. Therefore, only NAA/Cr, Glu/Cr and Ch/Cr ratios are shown in Figure 8.

The CV values did not exceed 31% for any of the reported locations and metabolites. The highest CV (31%) was for Glu/Cr in the basal ganglia location, which is a difficult region to quantify in general because of its proximity to the cerebrospinal fluid (CSF) in the ventricles.

DISCUSSION

The TEA-EPSI technique is shown to be a useful method to measure glutamate concentrations throughout the brain by quantifying PRESS-2D J (TE-averaged) spectra. In terms of coverage, the original TE-averaged SI sequence (17) was only capable of obtaining a single slice within the same acquisition time. From a signal perspective, a previously shown 3D TE-averaged SI

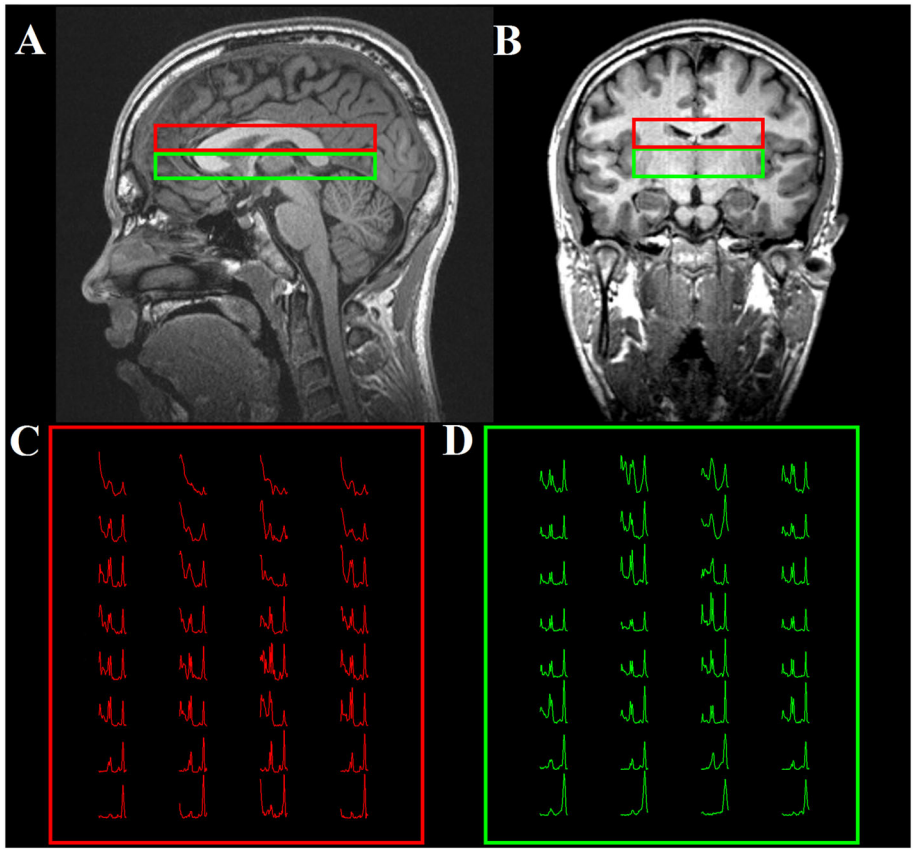

Figure 6. Individual spectral images are shown from two slices (C and D) from the same volunteer in Figure 5. Sagittal (A) and coronal (B) localizations are displayed for the two slices. The superior slice is displayed in red and the inferior slice is displayed in green for both the spatial localization and spectral display.

sequence (18) acquires only six t_1 points with two averages, which would yield a much lower theoretical SNR than TEA-EPSI. From the comparison between the 8× and time-equivalent phantom results, it is apparent that using NUS with reconstruction yields more consistent values of Glu. A proper SNR comparison was not performed due to the denoising effects of the reconstruction algorithm, which would inflate SNR values of the 8× results artificially.

In contrast to the previous TE-averaged methods, TEA-EPSI does not eliminate Gln signal completely, which may be due to the fact that different TE values are used for acquisition. TEA-EPSI instead utilizes TE-averaging to collapse the multiplets into singlets, which are adequately spaced apart as seen from the simulation in Figure 3. Due to the collapse of the multiplets, TE averaging has inherent line broadening. In order to ensure that the residual Gln signal did not affect Glu quantitation, Gln was removed from the basis set for an *in vivo* case and no changes were seen in the fit results. The T_2 chosen in the simulation for Glu and Gln played a role in the amplitude of the resulting TE-averaged spectrum. Using a different T_2 value for the simulation (180 ms) yielded different peak amplitudes, but similar peak locations and relative peak ratios (not shown). Therefore, it is not expected that T_2 values played a large role in the fitting process for Glu and Gln. However, this may be an issue when investigating different pathologies where the T_2 values of Glu or Gln are drastically altered.

With the current scan parameters, the voxel sizes were relatively large, allowing for more signal acquisition. However, the large voxel size of $1.5 \times 1.5 \times 1.5$ cm^3 made it difficult to classify a voxel as purely white or gray matter. By using the spatial location of the voxel, it was possible to determine whether a voxel was a majority of one or the other. Absolute metabolite concentrations were not obtained, but the relationship between Glu in white and gray matter voxels is similar to that previously reported (41,42,17). Table 4 displays the mean values of the Glu/Cr ratios for the TEA-EPSI results, as well as the ratios from two other sources (41,17). Since the raw numbers for all of the studies are not available, no standard deviation or CV values are displayed. By looking at these ratios, it is clear that the TEA-EPSI findings are similar to the findings from these two studies. Furthermore, comparing the ratios from TEA-EPSI with those in a recent review article that compiled glutamate quantitation results from several MRS studies shows good agreement with literature values (43).

The advantage of using MANGO over other, more complex fitting algorithms is that it is easily implemented after the post-processing steps in MATLAB. Without any user input, the program is able to quantify several voxels in a relatively short amount of time. Admittedly, because of the simplicity of the algorithm, it does not fit smaller metabolites as well as other existing packages (35–38,44) have reported. This inability to fit smaller peaks may also be attributed to the fact that TE averaging destroys many smaller metabolite signals through phase averaging. Metabolites with lower T_2 values may also be suppressed, since longer TE lines are incorporated into the averaging process. Even though MANGO quantitation of TEA-EPSI data does not appear useful for smaller metabolites, it

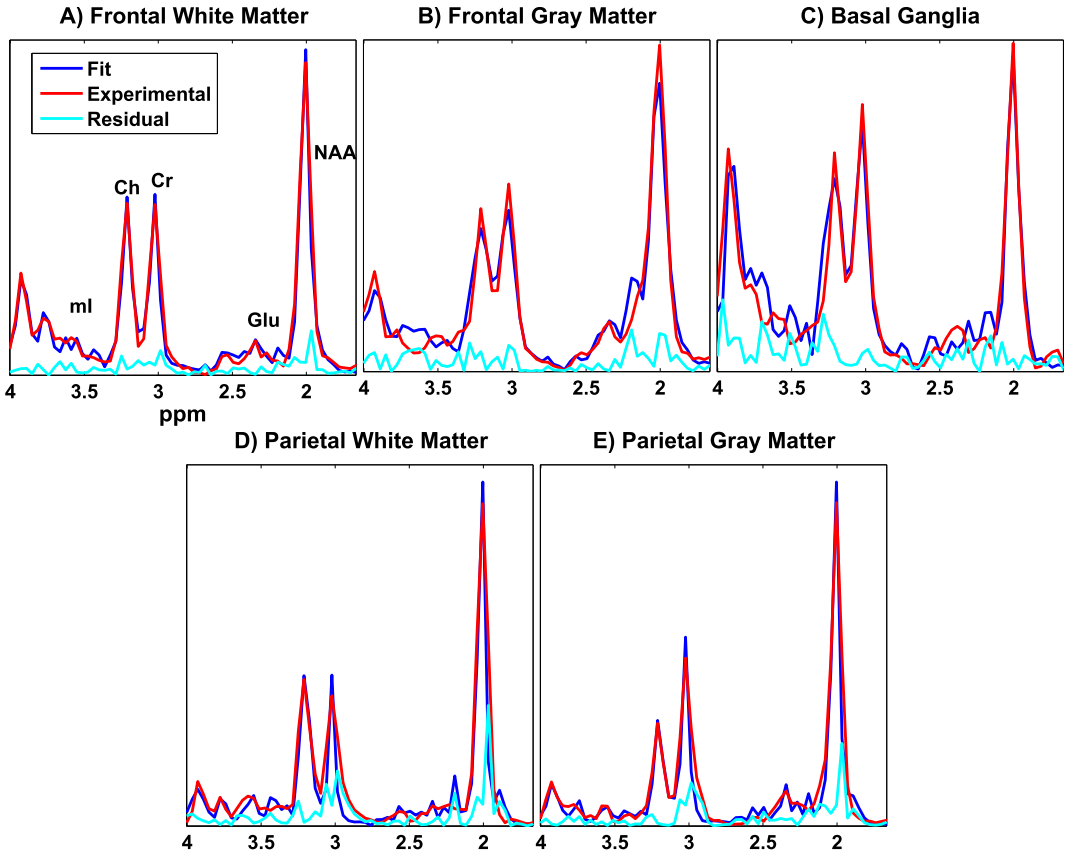

Figure 7. Spectra from (A) frontal white matter, (B) frontal gray matter, (C) basal ganglia, (D) parietal white matter and (E) parietal gray matter fitted with MANGO, along with residuals, are given for the healthy volunteer used in Figures 5, 6.

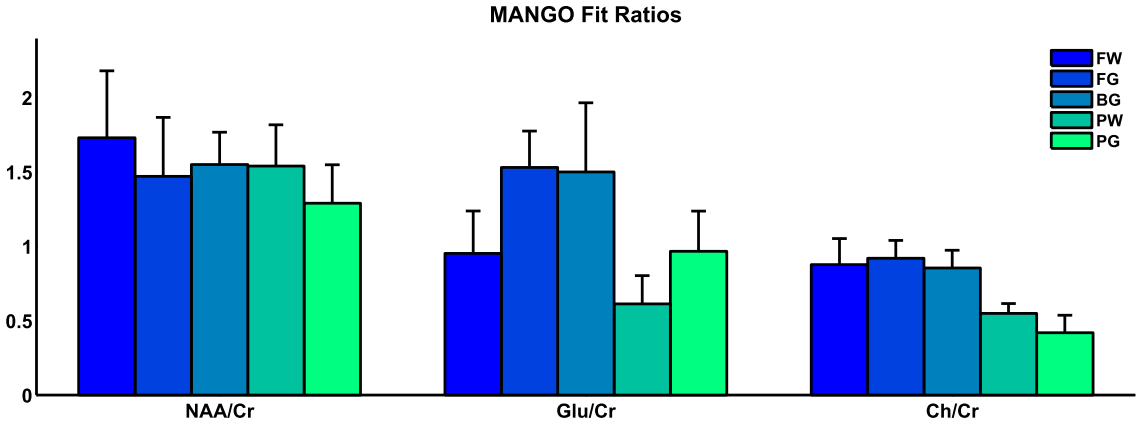

Figure 8. Quantitation results are shown using MANGO for the frontal white matter (FW), frontal gray matter (FG), basal ganglia (BG), parietal white matter (PW) and parietal gray matter (PG). MANGO scales all metabolites based on proton number.

is clear from the Monte Carlo simulation, phantom and *in vivo* results that MANGO is a good alternative for quantifying only NAA, Cr, Ch and Glu. Quantitation of mI was greatly influenced by the degree of water suppression and was difficult to measure reliably *in vivo* even with peak integration. The fitting technique of MANGO was good for demonstrating the reliability of glutamate detection using TEA-EPSI, however superior fitting algorithms exist for differentiating between control and patient groups, such as LCModel (35). It may be more appropriate to use these other, established algorithms for quantitation in pathological conditions, because these are more widely used and are already available in the literature for comparison purposes.

Fitting was greatly improved by utilizing prior knowledge for corrections before coil combination. Having F_2, F_1 frequency drift and phase corrections applied automatically based on the simulated singlet peaks (NAA, Cr and Ch) before coil addition ensured that peaks were added constructively. This was helpful, so that when the t_1 points were averaged only a line-broadening factor would have to be applied to the basis set in order to use MANGO for fitting. It is worth noting that if the number of coil elements is large, then this type of coil combination method could add a

Table 4. A comparison between Glu/Cr quantitation in white matter and gray matter using TEA-EPSI and two other references. All of the white and gray matter locations in (41) were averaged to show the mean Glu/Cr values, whereas (17) already provided the mean Glu/Cr information. Since raw numbers were not available for all the studies, standard deviations or coefficients of variance are not displayed.

Glu/Cr mean	Total white matter	Total gray matter
TEA-EPSI	0.78	1.25
Pouwels(41)	1.17	1.28
Srinivasan(17)	0.73	0.97

significant amount of time to post-processing. Currently, this method takes approximately 2–3 seconds per coil element for each voxel.

TE averaging is useful for detecting other metabolites as well (9–11). The TEA-EPSI technique can easily be modified to suit different purposes, with the caveat that ΔTE is constant and that the indirect spectral bandwidth is not too small. The reconstruction depends on the sparsity of the spectra in the transform domain (F_2, F_1) and a larger indirect spectral bandwidth helps to ensure that the spectra are more sparse. Implementing a different masking scheme to account for the total number of t_1 lines is necessary when modifying the sequence, but the reconstruction and post-processing steps would remain unchanged. Therefore, TEA-EPSI could be useful to quantify glycine (Gly) (9) and N-acetyl-aspartyl-glutamate (NAAG) (11) with minor adjustments. Alternatively, not all t_1 lines have to be included in the averaging process. Identifying the combination of t_1 lines from a certain TE range highlighting a metabolite of interest is possible (10). TEA-EPSI can be used to acquire this TE range and then only the optimal t_1 lines can be included in the averaging. This could be desirable when seeking to acquire multiple different TE-averaged spectra.

There are several improvements that can be made to the pulse sequence and some of these issues have been discussed previously (19). The spectral resolution in the direct dimension is currently suboptimal and only the major metabolites (NAA, Glx, Cr, Ch and mI) can be resolved easily. Since there is still a significant amount of signal at $t = 256$, zero-filling more than twice to improve resolution introduces ringing artifacts. This can affect fit results using packages such as LCModel, so sampling with 512 or more points will help resolve this issue. One of the main issues that is unfortunately common is lipid contamination, which occurs exclusively in voxels that are very close to the skull marrow. One solution is to use an inversion recovery pulse for lipid suppression (45). Another solution is to incorporate adiabatic pulses for volume localization (46,47) to help mitigate signal leakage from the skull marrow, as well as reduce CSDE. Although, due to the longer pulses an increased TE_{min} would have to be used, resulting in signal loss from T_2 decay. Another issue that needs to be addressed is inadequate water suppression in certain voxels. The seven-pulse water suppresion scheme (VAPOR) (48) has been shown to be very useful for this purpose and using these pulses may lead to more accurate quantitation of mI *in vivo*.

Quantitative comparisons between 1D PRESS and PRESS-2D J (49), as well as 2D JPRESS and PRESS-2D J (50), have already been performed. In addition, comparison between short TE MRSI and fully sampled TE-averaged MRSI (51,52) has also been discussed in the literature. These studies have shown that, while short TE STEAM or PRESS do not eliminate Gln signal, they still constitute a reliable method for Glu quantitation and may even be superior to the TE-averaged method. For the type of 3D spatial acquisition presented here, the TEA-EPSI technique would be able to average 64 t_1 lines, whereas a fully encoded, short TE MRSI scan would be able to average about 10 lines in 20 minutes. However, this does not mean that TEA-EPSI will outperform a short TE MRSI acquisition and a thorough comparison between the two methods using equal acquisition durations is necessary to determine which technique is better in assessing different patient groups. Prior-knowledge fitting (ProFit) (34,53) is a JPRESS quantitation algorithm capable of reporting metabolite concentrations reliably. ProFit uses the CRLB as a quality control metric and is capable of fitting the 2D JPRESS spectra from the 5D EP-JRESI technique. Understanding how CRLBs are affected by CS reconstruction is important before a quantitative comparison between the 5D EP-JRESI and TEA-EPSI methods can be made. A comparison between the two techniques is necessary in order to determine which method is preferable for investigating metabolites of interest. It may be possible to use these two methods in conjunction to understand certain pathologies better and this will be explored in a future study.

CONCLUSION

Accelerated TE-averaged echo planar spectroscopic imaging (TEA-EPSI) is a novel method incorporating non-uniform sampling and compressed sensing reconstruction in order to acquire TE-averaged spectra from three spatial dimensions (3D). Glutamate can be quantified using MANGO for prior-knowledge-based fitting. Differences between the white and gray matter voxels are in agreement with previous reports for healthy volunteers.

Acknowledgements

The authors acknowledge Dr. Brian L. Burns, Dr. Paul Macey and the National Institute of Health R21 Grant (NS080649-02).

REFERENCES

1. Brown T, Kincaid B, Ugurbil K. NMR chemical shift imaging in three dimensions. Proc. Natl. Acad. Sci. 1982; 79(11): 3523–3526.
2. Coyle JT, Puttfarcken P. Oxidative stress, glutamate, and neurodegenerative disorders. Sci. 1993; 262(5134): 689–695.
3. Sheldon AL, Robinson MB. The role of glutamate transporters in neurodegenerative diseases and potential opportunities for intervention. Neurochem. Int. 2007; 51(6): 333–355.
4. Greene JG, Greenamyre JT. Bioenergetics and glutamate excitotoxicity. Progr. Neurobiol. 1996; 48(6): 613–634.
5. Bleich S, Römer K, Wiltfang J, Kornhuber J. Glutamate and the glutamate receptor system: a target for drug action. Int. J. Geriatr. Psychiatry 2003; 18(S1): S33–S40.
6. Bottomley PA. Spatial localization in NMR spectroscopy in vivo. Ann. New York Acad. Sci. 1987; 508(1): 333–348.
7. Hurd R, Sailasuta N, Srinivasan R, Vigneron DB, Pelletier D, Nelson SJ. Measurement of brain glutamate using TE-averaged PRESS at 3 T. Magn. Reson. Med. 2004; 51(3): 435–440.
8. Ryner LN, Sorenson JA, Thomas MA. Localized 2D J-resolved 1 H MR spectroscopy: strong coupling effects in vitro and in vivo. Magn. Reson. Imaging 1995; 13(6): 853–869.
9. Prescot AP, de Frederick B, Wang L, Brown J, Jensen JE, Kaufman MJ, Renshaw PF. In vivo detection of brain glycine with echo-time-averaged 1 H magnetic resonance spectroscopy at 4.0 T. Magn. Reson. Med. 2006; 55(3): 681–686.

10. Prescot AP, Richards T, Dager SR, Choi C, Renshaw PF. Phase-adjusted echo time (PATE)-averaging 1 H MRS: application for improved glutamine quantification at 2.89 T. NMR Biomed. 2012; 25(11): 1245–1252.
11. Zhang Y, Li S, Marenco S, Shen J. Quantitative measurement of N-acetyl-aspartyl-glutamate at 3 T using TE-averaged PRESS spectroscopy and regularized lineshape deconvolution. Magn. Reson. Med. 2011; 66(2): 307–313.
12. Ernst T, Jiang CS, Nakama H, Buchthal S, Chang L. Lower brain glutamate is associated with cognitive deficits in HIV patients: A new mechanism for HIV-associated neurocognitive disorder. J. Magn. Reson. Imaging 2010; 32(5): 1045–1053.
13. Hancu I, Zimmerman EA, Sailasuta N, Hurd RE. 1H MR spectroscopy using TE averaged PRESS: a more sensitive technique to detect neurodegeneration associated with Alzheimer's disease. Magn. Reson. Med. 2005; 53(4): 777–782.
14. Srinivasan R, Sailasuta N, Hurd R, Nelson S, Pelletier D. Evidence of elevated glutamate in multiple sclerosis using magnetic resonance spectroscopy at 3 T. Brain 2005; 128(5): 1016–1025.
15. Chang L, Jiang CS, Ernst T. Effects of age and sex on brain glutamate and other metabolites. Magn. Reson. Imaging 2009; 27(1): 142–145.
16. Taylor MJ, Mannie ZN, Norbury R, Near J, Cowen PJ. Elevated cortical glutamate in young people at increased familial risk of depression. Int. J. Neuropsychopharmacol. 2011; 14(2): 255–259.
17. Srinivasan R, Cunningham C, Chen A, Vigneron D, Hurd R, Nelson S, Pelletier D. TE-averaged two-dimensional proton spectroscopic imaging of glutamate at 3 T. NeuroImage 2006; 30(4): 1171–1178.
18. Li Y, Chen AP, Crane JC, Chang SM, Vigneron DB, Nelson SJ. Three-dimensional J-resolved H-1 magnetic resonance spectroscopic imaging of volunteers and patients with brain tumors at 3 T. Magn. Reson. Med. 2007; 58(5): 886–892.
19. Wilson NE, Iqbal Z, Burns BL, Keller M, Thomas MA. Accelerated five-dimensional echo planar J-resolved spectroscopic imaging: Implementation and pilot validation in human brain. Magn. Reson. Med. 2016; 75(1): 42–51. doi: 10.1002/mrm.25605.
20. Mansfield P Spatial mapping of the chemical shift in NMR. Magn. Reson. Med. 1984; 1(3): 370–386.
21. Posse S, Tedeschi G, Risinger R, Ogg R, Bihan DL. High speed 1 H spectroscopic imaging in human brain by echo planar spatial-spectral encoding. Magn. Reson. Med. 1995; 33(1): 34–40.
22. Lustig M, Donoho D, Pauly JM. Sparse MRI: The application of compressed sensing for rapid MR imaging. Magn. Reson. Med. 2007; 58(6): 1182–1195.
23. Barna J, Laue E, Mayger M, Skilling J, Worrall S. Exponential sampling, an alternative method for sampling in two-dimensional NMR experiments. J. Magn. Reson. 1987; 73(1): 69–77.
24. Schmieder P, Stern AS, Wagner G, Hoch JC. Application of nonlinear sampling schemes to COSY-type spectra. J. Biomol. NMR 1993; 3(5): 569–576.
25. Kazimierczuk K, Zawadzka A, Koźmiński W. Optimization of random time domain sampling in multidimensional NMR. J. Magn. Reson. 2008; 192(1): 123–130.
26. Hyberts SG, Takeuchi K, Wagner G. Poisson-gap sampling and forward maximum entropy reconstruction for enhancing the resolution and sensitivity of protein NMR data. J. Am. Chem. Soc. 2010; 132(7): 2145–2147.
27. Smith S, Levante T, Meier BH, Ernst RR. Computer simulations in magnetic resonance. An object-oriented programming approach. J. Magn. Reson., Ser. A 1994; 106(1): 75–105.
28. Macura S, Brown LR. Improved sensitivity and resolution in two-dimensional homonuclear J-resolved NMR spectroscopy of macromolecules. J. Magn. Reson. 1983; 53(3): 529–535.
29. Schulte RF, Lange T, Beck J, Meier D, Boesiger P. Improved two-dimensional J-resolved spectroscopy. NMR Biomed. 2006; 19(2): 264–270.
30. Govindaraju V, Young K, Maudsley AA. Proton NMR chemical shifts and coupling constants for brain metabolites. NMR Biomed. 2000; 13(3): 129–153.
31. Ogg RJ, Kingsley R, Taylor JS. WET, a T1-and B1-insensitive water-suppression method for in vivo localized 1 H NMR spectroscopy. J. Magn. Reson., Ser. B 1994; 104(1): 1–10.
32. Goldstein T, Osher S. The split Bregman method for L1-regularized problems. SIAM J. Imaging Sci. 2009; 2(2): 323–343.
33. Klose U In vivo proton spectroscopy in presence of eddy currents. Magn. Reson. Med. 1990; 14(1): 26–30.
34. Fuchs A, Boesiger P, Schulte RF, Henning A. ProFit revisited. Magn. Reson. Med. 2014; 71(2): 458–468.
35. Provencher SW. Estimation of metabolite concentrations from localized *in vivo* proton NMR spectra. Magn. Reson. Med. 1993; 30(6): 672–679.
36. Wilson M, Reynolds G, Kauppinen RA, Arvanitis TN, Peet AC. A constrained least-squares approach to the automated quantitation of *in vivo* 1 H magnetic resonance spectroscopy data. Magn. Reson. Med. 2011; 65(1): 1–12.
37. Ratiney H, Sdika M, Coenradie Y, Cavassila S. Ormondt Dv, Graveron-Demilly D. Time-domain semi-parametric estimation based on a metabolite basis set. NMR Biomed. 2005; 18(1): 1–13.
38. Naressi A, Couturier C, Devos J, Janssen M, Mangeat C, DeBeer R, Graveron-Demilly D. Java-based graphical user interface for the MRUI quantitation package. Magn. Reson. Mater. Phys. Biol. Med. 2001; 12(2–3): 141–152.
39. Boyd S, Vandenberghe L. *Convex Optimization*. Cambridge University Press: Cambridge; 2004.
40. Cavassila S, Deval S, Huegen C, VanOrmondt D, Graveron-Demilly D. Cramer–Rao bounds: an evaluation tool for quantitation. NMR Biomed. 2001; 14(4): 278–283.
41. Pouwels PJ, Frahm J. Regional metabolite concentrations in human brain as determined by quantitative localized proton MRS. Magn. Reson. Med. 1998; 39(1): 53–60.
42. McLean MA, Woermann FG, Barker GJ, Duncan JS. Quantitative analysis of short echo time 1 H-MRSI of cerebral gray and white matter. Magn. Reson. Med. 2000; 44(3): 401–411.
43. Ramadan S, Lin A, Stanwell P. Glutamate and glutamine: a review of *in vivo* MRS in the human brain. NMR Biomed. 2013; 26(12): 1630–1646.
44. Chong DG, Kreis R, Bolliger CS, Boesch C, Slotboom J. Two-dimensional linear-combination model fitting of magnetic resonance spectra to define the macromolecule baseline using FiTAID, a Fitting Tool for Arrays of Interrelated Datasets. Magn. Reson. Mater. Phys. Biol. Med. 2011; 24(3): 147–164.
45. Spielman DM, Pauly JM, Macovski A, Glover GH, Enzmann DR. Lipid-suppressed single-and multisection proton spectroscopic imaging of the human brain. J. Magn. Reson. Imaging 1992; 2(3): 253–262.
46. Garwood M, DelaBarre L. The return of the frequency sweep: designing adiabatic pulses for contemporary NMR. J. Magn. Reson. 2001; 153(2): 155–177.
47. Scheenen TW, Klomp DW, Wijnen JP, Heerschap A. Short echo time 1 H-MRSI of the human brain at 3 T with minimal chemical shift displacement errors using adiabatic refocusing pulses. Magn. Reson. Med. 2008; 59(1): 1–6.
48. Tkáč I, Starčuk Z, Choi IY, Gruetter R. In vivo 1 H NMR spectroscopy of rat brain at 1 ms echo time. Magn. Reson. Med. 1999; 41(4): 649–656.
49. Wijtenburg SA, Knight-Scott J. Very short echo time improves the precision of glutamate detection at 3 T in 1 H magnetic resonance spectroscopy. J. Magn. Reson. Imaging 2011; 34(3): 645–652.
50. Gonenc A, Govind V, Sheriff S, Maudsley A. Comparison of spectral fitting methods for overlapping J-coupled metabolite resonances. Magn. Reson. Med. 2010; 64(3): 623–628.
51. Yung K, Tsai S, Lin F, Henry P, Yoshimoto A, Posse S. Comparison of TE-averaged with short TE Proton-Echo-Planar-Spectroscopic-Imaging (PEPSI) for mapping glutamate in human brain. In *Proc. 18th Annual Meeting of ISMRM, Honolulu, Hawaii*; 2009; abstract 4314.
52. Posse S, Otazo R, Dager SR, Alger J. MR spectroscopic imaging: principles and recent advances. J. Magn. Reson. Imaging 2013; 37(6): 1301–1325.
53. Schulte RF, Boesiger P. ProFit: two-dimensional prior-knowledge fitting of J-resolved spectra. NMR Biomed. 2006; 19(2): 255–263.